Research Article

Xuemei Zhang, Peng Zhang*, Tingya Wang, Ying Zheng, Linhong Qiu, and Siwen Sun

# Compressive strength and anti-chloride ion penetration assessment of geopolymer mortar merging PVA fiber and nano-$SiO_2$ using RBF–BP composite neural network

https://doi.org/10.1515/ntrev-2022-0069
received November 27, 2021; accepted January 26, 2022

**Abstract:** In this study, we investigated the mechanical properties and chloride ion permeation resistance of geopolymer mortars based on fly ash modified with nano-$SiO_2$ (NS) and polyvinyl alcohol (PVA) fiber and metakaolin (MK) at dose levels of 0–1.2% for PVA fiber and 0–2.5% for NS. The Levenberg–Marquardt (L–M) back propagation (BP) neural network, as well as the radial-based function (RBF) neural network, was used to predict the compressive strength and chloride ion permeation resistance of the geopolymer mortar with different admixtures of nanoparticles and PVA fiber, wherein the electric flux value was used as the index for chloride ion permeation performance. The RBF–BP composite neural network was constructed to study the compressive strength and chloride ion permeation resistance of nanoparticle-doped and PVA fiber ground geopolymer mortars. According to the experimental results of the RBF–BP composite neural network model, the mean square error (MSE) was observed to be 0.00071943, root mean square error (RMSE) was 0.026822, and mean absolute error (MAE) was 0.026822, thereby showing higher prediction accuracy, faster convergence, and better fitting effect compared with the single BP neural network and RBF neural network models. In this study, we combined the RBF–BP composite artificial neural network, providing a new method for the future assessment of the compressive strength and chloride ion penetration resistance of geopolymer mortar merging PVA fibers and NS in experiments and engineering studies.

**Keywords:** geopolymer mortar, RBF–BP composite neural network, resistance to chloride ion penetration, compressive strength, prediction

*** Corresponding author: Peng Zhang,** School of Water Conservancy Engineering, Zhengzhou University, Zhengzhou, 450001, China, e-mail: zhangpeng@zzu.edu.cn
**Xuemei Zhang, Tingya Wang, Ying Zheng, Linhong Qiu, Siwen Sun:** School of Water Conservancy Engineering, Zhengzhou University, Zhengzhou, 450001, China

## 1 Introduction

With rapid population growth and damaged infrastructure, increasing attention is being focused on the construction industry. Cement-based materials are one of the most widely used materials in the construction industry globally [1]. Most cement-based materials use silicate cement (OPC) as a binder [2], and cement is produced from two different sources of carbon dioxide, with rotary kilns operated *via* fossil fuel combustion being the largest source and the chemical process of calcining limestone into lime, which is also produced by cement kilns [3]. The OPC releases almost equal amounts of carbon dioxide during its production. Data from the US Geological Survey show that since 2013, approximately 4 billion tons of polyester cement have been produced annually, accounting for 8% of the total global carbon dioxide emissions. With the rapid growth of the global economy, it is estimated that in the next 30 years, cement output will increase to approximately 5 billion tons globally [4]. Such massive emissions of carbon dioxide have caused serious environmental pollution and has brought about huge social pressure. Many researchers are beginning to look for materials that save energy and are environmentally friendly, for example, Golewski discovered plain concretes prepared based on a quaternary binder to reduce carbon dioxide emissions [5]. In addition, cement-based materials have serious dissolution problems that affect the strength and durability of buildings [6]. Therefore, there is an urgent need for an energy-saving and environmentally friendly alternative material to fundamentally solve this problem [7,8]. As a potential alternative to cement, geopolymers have demonstrated many advantages such as excellent mechanical

properties, high temperature resistance, corrosion resistance, and low energy consumption in production owing to their unique three-dimensional mesh structure [9,10].

Chithambaram *et al.* [11] explored the thermodynamic phenomena of geopolymer mortar and showed that it exhibited a change from crystalline to amorphous state above 600°C. Bingol *et al.* [12] explored the thermodynamic phenomena of geopolymer mortars and compared the durability of slag geopolymer mortars with cement mortars and observed that the durability of slag geopolymer mortars was considerably higher than that of cement mortars. Elyamany *et al.* [13] showed that geopolymer mortars were more resistant to magnesium sulfate attacks than ordinary silicate cement mortars. Owing to the defects of slow curing, high porosity, and slow strength development of geopolymers, in recent years, domestic and foreign scholars have added nano-$SiO_2$ (NS) to geopolymers to improve the densification of geopolymers and concrete, which in turn improves the mechanical properties [14–16], durability [17,18], rheological properties [19], and post-high-temperature mechanical properties [20]. Zidi *et al.* [21] synthesized NS partially based geopolymers and discovered that the mechanical strength of the geopolymer was improved by adding a moderate amount of NS. Phoongernkham *et al.* [22] improved the bond strength between the concrete matrix and the geopolymer. NS not only improves the properties of geopolymer mortar but also exhibits superiority of low cost and excellent performance. Therefore, adding NS to geopolymer mortar is in line with the scientific basis.

Owing to the low flexural and tensile strengths of geopolymer mortars, the addition of certain fibers such as steel fibers [23], polyvinyl alcohol (PVA) fibers, and polypropylene fibers [24] to geopolymer mortars can improve the toughness and enhance their durability performance as shown in relevant domestic and international studies. Among them, PVA fiber demonstrates excellent qualities such as high strength, high modulus of elasticity, wear resistance, acid and alkali resistance, good weather resistance, among others, and are non-toxic, non-polluting, and non-damaging to human skin and harmless to human body, which is one of the new generation of high-tech green building materials [25]. Xu *et al.* [26] showed that PVA fibers can enhance the toughness and denseness of fly ash geopolymer composites and improve their bonding, and Malik *et al.* [27] observed that PVA fibers could enhance the strength and durability of geopolymers; simultaneously, it was observed that PVA fiber and NS materials could significantly reduce the explosion spalling of geopolymers. The properties of geopolymer mortar can be effectively improved by adding NS and PVA fibers [28,29].

China is a vast country, and materials such as concrete face a variety of service environments, of which saline environments are one of the most common. China has a large number of marine and offshore projects, where structures are susceptible to damage owing to the harsh marine environment with complex multi-field coupling effects such as waves, tides, dry and wet cycles, and salt [30–32]. In coastal, marine, and offshore areas, the presence of chlorides can easily lead to severe deterioration of reinforced concrete structures and high maintenance costs [33]. Geopolymer mortars are more resistant to chloride ion penetration and have greater corrosion protection than cement mortars [33,34]. The use of geopolymer mortar for engineering construction can not only save costs, save energy, and protect the environment but also enhance the durability of the building [35]. Therefore, studying the chloride ion permeability resistance of geopolymer mortars with NS and PVA fibers is necessary.

With developments in artificial intelligence, various properties of construction materials have been predicted using machine learning. Golewski [36,37] proposed digital image correlation technology to test the fracture performance of fly ash concrete and achieved good results. Owing to the diverse composition of building materials, conducting experiments on each of them is not possible, so the prediction of unknown data is often made using artificial neural network models based on existing data. Nagajothi and Elavenil [38] used an artificial neural network (ANN) model to predict the mechanical properties of aluminum silicate on geopolymer concrete, and the results showed that the prediction results of the ANN were in good agreement with the experimental results. Rahman and Al-Ameri [39] proposed an ANN model to assess the bond behavior of self-compacting geopolymer concrete with basaltic fiber reinforced plastics (FRP) bars. The ANN predicted all properties of cement mortar [40–42], geopolymer concrete [43–46], and geopolymer mortar [47,48]. Li *et al.* [49] explored that radial-based function–back propagation (RBF–BP) neural network that can identify the membership of six common basic patterns of shape defects. Liu [50] realized fault attribute classification and fault diagnosis of building electrical system by using RBF–BP neural network. However, there are few studies on the properties of geopolymer mortars merging PVA fibers and NS at home and abroad, and there are no suitable prediction methods and models for the prediction of compressive strength and chloride ion permeability of geopolymer mortars merging PVA fibers and

NS. Therefore, in this study, the proposed RBF–BP composite neural network model is crucial for the prediction of the compressive strength and chloride ion permeability of geopolymer mortar merging PVA fibers and NS. The RBF–BP composite neural network can provide guidance for further experiments and engineering studies on the mechanical properties and chloride ion permeation resistance of geopolymer mortars merging PVA fibers and NS.

## 2 Experiment program

The objective of this investigation is to explore the effect of different amounts of $SiO_2$ nanoparticles and PVA fibers on the compressive strength and chloride ion penetration resistance of geopolymer mortars. When designing the proportion of geopolymer mortar with NS and PVA fibers, the control variable method was used, that is, fixing the water–binder ratio, cement–sand ratio, water–glass modulus, and excitation ratio (the ratio of alkaline exciter to cementitious material), while varying the amount of NS or PVA fibers.

The NS, a loose white powder, has a content of 99.7%, with an average particle size of 30 nm produced by Hangzhou Wanjing New Materials Co. The PVA fiber, with the compressive strength of 1,560 MPa, has a diameter of 40 μm, standard length of 12 mm, and elongation of 6.5%. The metakaolin concludes 54% $SiO_2$ and 43% $Al_2O_3$, and the margin of error is 2%. Besides, the metakaolin contains less than 1.3% $Fe_2O_3$, 0.8% CaO and MgO, and 0.7% $K_2O$ and $Na_2O$. The fly ash whose water absorbing capacity is 105% has the bulk density of 0.77 g/cm$^3$, standard consistency of 47.1%, and specific gravity of 2.16 g/cm$^3$. The test mix design was carried out with reference to the literature [51,52], and the parameters of the mix were finally determined through trial mixing as follows: water–binder ratio (the ratio of water contained in the added water and alkali exciter to cementitious material) of 0.65, cement–sand ratio of 1:1, 30% fly ash, and 70% metakaolin as raw material for silica-aluminate, and alkali exciter solution comprising solid sodium hydroxide, sodium silicate solution, and water. The modulus of water glass was decreased from 3.2 to 1.3 by adding sodium hydroxide and then an appropriate amount of water was added to adjust the mass fraction of sodium oxide to 15%, referring to the water–glass modulus adjustment and calculation proposed by other researcher [53]. NS and PVA fibers were incorporated in two forms: single and compound. The NS and PVA fibers were incorporated into the compounded geopolymer mortar, where the NS dose was fixed at 1.0% and the PVA fiber dose was 0.2, 0.4, 0.6, 0.8, 1.0, or 1.2% when the PVA fiber dose was changed [54]; when the NS dose was changed, the PVA fiber dose was fixed at 0.6% and the NS dose was 0.5, 1.0, 1.5, 2.0, or 2.5%.

To assess the resistance to chloride ion permeation of geopolymer mortars with $SiO_2$ and PVA fibers, we herein use the electrical flux method for the chloride ion

**Table 1:** Mix proportions of geopolymer mortar for train set [32]

| Mix no. | Water | Metakaolin | Fly ash | Quartz sand | Water glass | NaOH | PVA fiber | NS | Water-reducing agents | Compressive strength | Electric flux values |
|---|---|---|---|---|---|---|---|---|---|---|---|
| | kg/m$^3$ | kg/m$^3$ | kg/m$^3$ | kg/m$^3$ | kg/m$^3$ | kg/m$^3$ | % | % | kg/m$^3$ | MPa | C |
| 1 | 106.2 | 429.5 | 184.1 | 613.6 | 445.4 | 71 | 0 | 0 | 3.07 | 44.2 | 1426.31 |
| 2 | 106.2 | 429.5 | 184.1 | 613.6 | 445.4 | 71 | 0.2 | 0 | 3.07 | 50.8 | 1294.38 |
| 3 | 106.2 | 429.5 | 184.1 | 613.6 | 445.4 | 71 | 0.4 | 0 | 3.07 | 55.3 | 1216.08 |
| 4 | 106.2 | 429.5 | 184.1 | 613.6 | 445.4 | 71 | 0.6 | 0 | 3.07 | 58.5 | 1185.84 |
| 5 | 106.2 | 429.5 | 184.1 | 613.6 | 445.4 | 71 | 0.8 | 0 | 3.07 | 60.3 | 1150.24 |
| 6 | 106.2 | 429.5 | 184.1 | 613.6 | 445.4 | 71 | 1.0 | 0 | 3.07 | 50.5 | 1158.52 |
| 7 | 106.2 | 429.5 | 184.1 | 613.6 | 445.4 | 71 | 1.2 | 0 | 3.07 | 48.1 | 1195.41 |
| 8 | 106.2 | 427.2 | 183.1 | 613.6 | 445.4 | 71 | 0 | 0.5 | 3.07 | 45.0 | 1220.82 |
| 9 | 106.2 | 425.0 | 182.2 | 613.6 | 445.4 | 71 | 0 | 1.0 | 3.07 | 47.3 | 1185.06 |
| 10 | 106.2 | 422.7 | 181.2 | 613.6 | 445.4 | 71 | 0 | 1.5 | 3.07 | 50.1 | 1121.13 |
| 11 | 106.2 | 420.4 | 180.2 | 613.6 | 445.4 | 71 | 0 | 2.0 | 3.07 | 48.8 | 1164.84 |
| 12 | 106.2 | 418.1 | 179.2 | 613.6 | 445.4 | 71 | 0 | 2.5 | 3.07 | 46.4 | 1190.52 |
| 13 | 106.2 | 429.5 | 182.2 | 613.6 | 445.4 | 71 | 0.2 | 1.0 | 3.07 | 53.9 | 1147.62 |
| 14 | 106.2 | 429.5 | 182.2 | 613.6 | 445.4 | 71 | 0.4 | 1.0 | 3.07 | 57.4 | 1107.48 |
| 15 | 106.2 | 429.5 | 182.2 | 613.6 | 445.4 | 71 | 0.8 | 1.0 | 3.07 | 62.4 | 1071.78 |
| 16 | 106.2 | 429.5 | 182.2 | 613.6 | 445.4 | 71 | 1.0 | 1.0 | 3.07 | 55.7 | 1076.94 |

permeation test that visually and accurately assesses the chloride ion resistance of geopolymer mortars by testing the electrical flux values. Conversely, the lower the measured flux value, the better is the resistance of the mortar to chloride ions. The specific dosage and mix of each material are listed in Table 1.

# 3 Model establishment

An RBF–BP composite neural network with a BP neural network and RBF neural network was used to predict the compressive strength and resistance to chloride ion penetration of geopolymer mortar merging PVA fiber and NS by combining fly ash, water, alkali exciter, metakaolin, quartz sand, water-reducing agent, NS, and PVA fiber dosing parameters.

Herein the NS and PVA fibers are the main objects of our study; however, because NS will replace fly ash with equal mass and simultaneously affect the amount of kaolinite added, four material parameters affecting the compressive strength and chloride ion penetration resistance of the geopolymer mortar, namely, NS admixture, PVA fiber admixture, kaolinite admixture, and fly ash admixture, are finally chosen as input parameters, so each neural network of the input layer has four neurons. In the compressive strength experiment, the compressive strength value was chosen as the output parameter. As the electric flux method is used as the experimental method in the chloride ion penetration resistance experiment, the processed electric flux value was chosen as the output parameter. Therefore, for each experiment, the output layer was 1. In the training process, 70% of the sample data were set as the training set data, and the remaining 30% was the prediction set data.

## 3.1 BP neural network

On the basis of the error back propagation algorithm, the BP neural network is a multi-layer feed-forward neural network composed of an import layer, one or more intermediate layers, and an export layer. In each layer, the number of neurons relies on a specific analysis of the problem.

Owing to slow convergence, low learning efficiency, and difficulty in deciding the number of intermediate layers and their neurons, as well as easily falling into local minima of the traditional BP neural network, we herein adopt the improved Levenberg–Marquardt BP neural network. As a three-layer BP neural network was proven to theoretically achieve any complex nonlinear mapping, a BP neural network whose hidden layer is one which can meet most prediction requirements. The number of neurons in the implicit layer can be derived from the following equation [55]:

$$m = (n + l)^{\frac{1}{2}} + a, \tag{1}$$

$$m = 2n + 1, \tag{2}$$

$$m = \log_2 n, \tag{3}$$

where $m$, $n$, and $l$ denote the number of neurons. $m$ is in the hidden layer, $n$ is in the input layer, $l$ is in the output layer, and $a$ is the constant $a = 1–10$.

The above equation can calculate the range of the number of neurons in the implicit layer, but a specific and precise value cannot be obtained, and several experiments are needed to combine the prediction accuracy and convergence; finally, the number of neurons is set to eight.

In this study, the excitation function of the implicit layer selects the tansig function, the output layer transfer function uses the purelin function, and the reverse training uses the trainlm gradient descent method. Suppose that the $i$th neuron in the model has input values $X_1$, $X_2$, $X_3$,..., $X_n$ and the corresponding weights are $W_1$, $W_2$, $W_3$,...,$W_n$, $Y_i$, can be derived from the following equation:

$$Y_i = f\left(\sum_{i=0}^{n} X_i \times W_i\right), \tag{4}$$

where $f$ is the excitation function, and $Y_i$ represents the output value. In the Levenberg–Marquardt algorithm, the values of the weight matrix of multiple neurons are distributed between $(-1, 1)$, which is determined by the weight adjustment formula.

$$W_{i+1} = W_i - (J^T J + \mu I)^{-1} J^T e. \tag{5}$$

However, when using the weight adjustment formula, assigning initial values to the weight matrix is necessary; in this study, the weight matrix is initialized using a random number generation method. As the BP neural network is trained and learned, the error between the output and the real result becomes increasingly small. For the purpose of making the BP neural network model training effect more accurate, the mean square error was selected as $10^{-7}$, and to avoid too slow convergence, the upper limit of the iterations number was set as 10,000. Generally speaking, the larger the learning rate, the faster is the convergence speed; however, a larger learning rate is likely to cause oscillations in the convergence process,

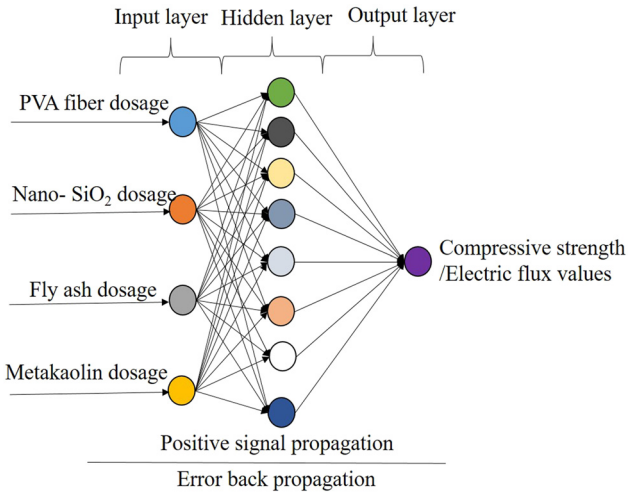


**Figure 1:** Structure of BP neural network.

resulting in an increase in the number of iterations, whereas a smaller learning rate will extend the training time and cannot guarantee that the error value of the network jumps out of the minima and eventually converges to the minimum error. After several training sessions, it was observed that when set to 0.5, the learning rate was optimal. The BP neural network structure can be displayed in Figure 1, and the set of parameters for the final constructed BP neural network are listed in Table 2.

## 3.2 RBF neural network

The RBF neutral network is a feed-forward neural network that includes a single implicit layer, and the topology of the RBF neural network is similar to that of BP, which comprises three layers. The input layer only transmits the input signal without transforming the input information and maps the input data directly to the hidden layer. The radial basis function, including inverse multi-quadratic functions, Gaussian functions, multi-quadratic functions, among others, is the excitation function in the hidden layer, which responds to the local signal and produces a larger output [56]. The output layer then acts in response to the action of the input pattern. The mapping from the input to output of the RBF neural network structure is nonlinear, while the mapping from the implicit layer to the output layer is linear [57]. Hartman *et al.* [58] observed that there are enough neurons in the implicit layer, and RBF neural networks can approximate any continuous function with arbitrary accuracy.

Owing to its simple form, the excitation function for neurons in the implicit layer chooses a Gaussian function, and its formula is shown in equation (6).

$$\varphi_i(x) = \exp\left(-\frac{||x - c_i||^2}{2\sigma_i^2}\right), \quad i = 1, 2, 3, \ldots, h, \tag{6}$$

where $x$ denotes the $n$-dimensional input vector, $c_i$ is the center of the $i$th radial basis function, $\sigma_i$ is the expansion constant, $h$ denotes the number of neurons in the implicit layer, and $||x - c_i||$ denotes the Euclidean distance between $x$ and $c_i$.

The learning algorithm of RBF neural network needs to solve three types of problems: first, determination of the neuron numbers for the implicit layer and RBF centers; second, selection of the expansion constants; and third, the weight matrix adjustment from the implicit layer space to the output space. The neurons in the implicit layer of regularized neural networks are sample inputs; in this study, this number was 4. Radial basis function centers are determined by self-organized learning, supervised selection, least squares, and random selection methods [59]. The extension constant selection is calculated using equation (7). The weights of the implied layer space and the output space are calculated using the least-squares method and are given in equation (8).

$$\sigma_i = \frac{c_{\max}}{\sqrt{2h}}, \quad h = 1, 2, 3, \ldots, h, \tag{7}$$

$$w = \exp\left(\frac{h}{c_{\max}^2}||x - c_i||\right), \quad h = 1, 2, 3, \ldots, h, \quad p = 1, 2, 3, \ldots, P, \tag{8}$$

where $c_{\max}$ denotes the maximum distance between the chosen centers.

To increase the comparability of the BP and RBF neural networks, the upper iteration limit, target error, and learning rate were kept the same as those of the BP

**Table 2:** BP neural network parameters

| Parameters | Hidden layer neurons | Hidden layer transfer function | Output layer transfer function | Target error | Iteration limit | Learning rate |
|---|---|---|---|---|---|---|
| Value | 8 | Tansig | Purelin | $10^{-7}$ | 10,000 | 0.5 |

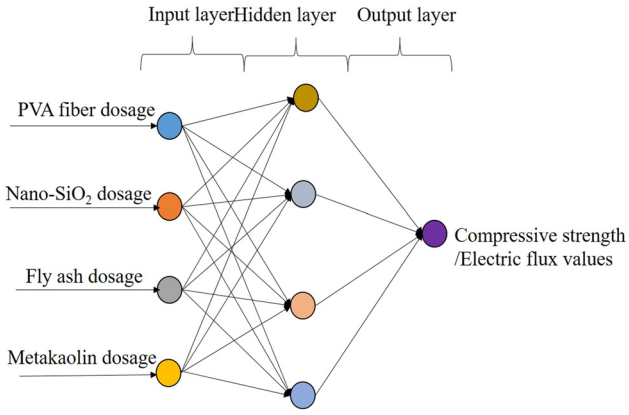


**Figure 2:** Structure of RBF neural network.

neural network. The RBF neural network structure can be displayed in Figure 2, and the set of parameters of the final constructed RBF neural network are listed in Table 3.

## 3.3 RBF–BP composite neural network

Both the RBF and BP neural network have their own characteristics. Complex nonlinear mapping can be realized by a BP neural network, whose disadvantages are low learning efficiency, slow convergence speed, and susceptibility to local minima in the learning process, and the determination of the neural network structure is extremely blind. The RBF neural network compensates for the defects in the BP neural network, but the mapping from the implicit layer to the output layer can only be linear. Under nonlinear conditions, the prediction results are more biased and the network generalization ability is poor [60]. Therefore, combining these two types of neural network structures can promote the respective defects of the BP and RBF neural network. Based on the above, an RBF–BP composite neural network has been proposed, wherein the two networks are organically combined to form a composite neural network with two hidden layers comprising a BP subnet and an RBF subnet. The excitation function of the first implicit layer, which is a Gaussian function, is consistent with that of the RBF neural network, and the excitation function of the second implicit layer, using a sigmoid-type function, is consistent with that of the BP neural network. The RBF–BP composite neural network not only solves the shortcomings of slow convergence and low learning efficiency of the BP neural network model but also improves the performance of the RBF neural network. The RBF–BP composite neural network not only solves the problems of low learning efficiency and slow convergence of the BP neural network but also improves the problem that the RBF neural network cannot make like nonlinear predictions and enhances the

**Table 3:** RBF neural network parameters

| Parameters | Hidden layer neurons | Hidden layer transfer function | Output layer transfer function | Target error | Iteration limit | Learning rate |
|---|---|---|---|---|---|---|
| Value | 4 | Gauss | Linear | $10^{-7}$ | 10,000 | 0.5 |

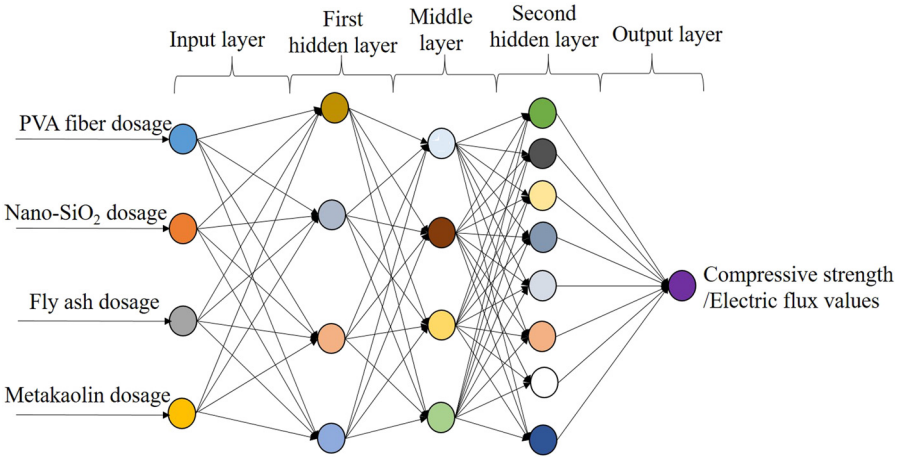


**Figure 3:** Structure of RBF–BP composite neural network.

nonlinear fitting ability, and the final obtained RBF–BP composite neural network has more network generalization ability and higher prediction accuracy.

The parameters of the RBF–BP composite neural network model, including the learning rate, upper limit of iteration number, and target error, are consistent with those of the other two types of neural network models. The RBF–BP composite neural network structure is displayed in Figure 3, and the set of parameters of the final RBF–BP composite neural network are listed in Table 4.

**Table 4:** RBF–BP composite neural network parameters

| Parameters | First layer of hidden layer neurons | Second layer of hidden layer neurons | First hidden layer excitation function | Second hidden layer excitation function | Output layer transfer function | Target error | Iteration limit | Learning rate |
|---|---|---|---|---|---|---|---|---|
| Value | 4 | 8 | Gauss function | Tansig | Purelin | $10^{-7}$ | 10,000 | 0.5 |

# 4 Model training and result analysis

On the basis of determining the research method and training model, 70% of the sample data used the model to train, and after the model was trained, the remaining 30% of the sample data was used for testing and the test results were analyzed and evaluated, and the test set data are shown in Table 5.

## 4.1 Network training and testing methods

The six sets of data above were learned and trained by training the three types of neural network models to predict the compressive strength and chloride ion penetration resistance of the nanoparticle-doped PVA fiber in the geopolymer mortar.

To avoid the influence of the absolute size and units of the sample data of the training results and facilitate subsequent data processing, the sample data were normalized before applying the sample data, and the data were mapped to between [–1,1] [61]. Simultaneously, before the model is trained and the training results are output, the output data are normalized back to the original value interval. The inverse normalization formula for the input and output data can be calculated using equation (9).

$$Y_{\text{predict}} = (Y_{\text{predict,nor}} + 1)Y_{\max} - Y_{\text{predict,nor}}Y_{\min}, \quad (9)$$

where $Y_{\text{predict}}$ is the normalized model prediction result, and $Y_{\text{predict,nor}}$ is the inverse normalized model prediction result.

First, the neural network model was applied to train 16 sets of experimental data. Subsequently, the trained neural network was used to predict the remaining six sets of data. Finally, the training results were compared and analyzed with real results.

**Table 5:** Mix proportions of geopolymer mortar for test set

| Mix no. | Water | Metakaolin | Fly ash | Quartz sand | Water glass | NaOH | PVA fiber | Nano -$SiO_2$ | Water-reducing agents | Compressive strength | Electric flux values |
|---|---|---|---|---|---|---|---|---|---|---|---|
| | kg/m³ | kg/m³ | kg/m³ | kg/m³ | kg/m³ | kg/m³ | % | % | kg/m³ | MPa | C |
| 1 | 106.2 | 429.5 | 182.2 | 613.6 | 445.4 | 71 | 1.2 | 1.0 | 3.07 | 54.1 | 1102.36 |
| 2 | 106.2 | 429.5 | 183.1 | 613.6 | 445.4 | 71 | 0.6 | 0.5 | 3.07 | 59.1 | 1157.88 |
| 3 | 106.2 | 429.5 | 182.2 | 613.6 | 445.4 | 71 | 0.6 | 1.0 | 3.07 | 61.1 | 1096.02 |
| 4 | 106.2 | 429.5 | 181.2 | 613.6 | 445.4 | 71 | 0.6 | 1.5 | 3.07 | 63.6 | 1055.16 |
| 5 | 106.2 | 429.5 | 180.2 | 613.6 | 445.4 | 71 | 0.6 | 2.0 | 3.07 | 62.3 | 1107.06 |
| 6 | 106.2 | 429.5 | 179.2 | 613.6 | 445.4 | 71 | 0.6 | 2.5 | 3.07 | 59.7 | 11566.98 |

## 4.2 Experimental results and analysis

Developing a set of practical evaluation indicators to comprehensively measure the performance of the three types of neural networks is necessary. According to the evaluation principles and practices, we herein selected mean square error (MSE), root mean square error (RMSE), and mean absolute error (MAE) as the evaluation indicators. MSE:

$$\mathrm{MSE} = \frac{1}{n}\sum_{i=1}^{n}(o_i - t_i)^2. \tag{10}$$

RMSE:

$$\mathrm{RMSE} = \sqrt{\frac{\sum_{i=1}^{n}(o_i - t_i)^2}{n}}. \tag{11}$$

MAE:

$$\mathrm{MAE} = \frac{1}{n}\sum_{i=1}^{n}|o_i - t_i|. \tag{12}$$

In the above three equations, $n$ is the sample size, $t_i$ is the model-predicted value, and $o_i$ is the true value.

The compressive strength and resistance to chloride ion permeability predicted from the three types of neural networks were compared with the experimental values, and the comparison results are shown in Figures 4 and 5.

The predicted results in Figures 4 and 5 show the effect of $SiO_2$ nanoparticles and PVA fibers on the compressive strength and chloride ion penetration resistance of the geopolymer mortar. When the NS content was 1.5%, the compressive strength of the geopolymer mortar was the highest, which is generally consistent with previous studies where the optimum NS content in geopolymer mortars was predicted to be between 1.0% and 2.0% [22,62]. However, unlike the optimum $SiO_2$ content in cement mortar and concrete [63,64], the geopolymer mortar showed optimum resistance to chloride ion penetration as the dosage of PVA fiber was 0.6% and the NS content was 1.0%. NS increases its hydration and makes the geopolymer mortar denser owing to its high reactivity [65,66], reducing the porosity of the material during geopolymer hardening and increasing its density, which in turn leads to a denser structure and reduced micro-cracking [67–69]. These results are in general agreement with those of previous studies [70,71].

The predictions obtained from three neural network models were all close to the experimental values. However, from the fitting effect, the RBF–BP neural network outperforms the other two types of neural networks, and the BP neural network fits the worst, indicating that the RBF–BP neural network has better generalization ability and approximates the true results more accurately. In terms of errors, all three neural networks had small errors and met the prediction requirements. By comparing the evaluation indices of three types of neural networks, the results are presented in Table 6.

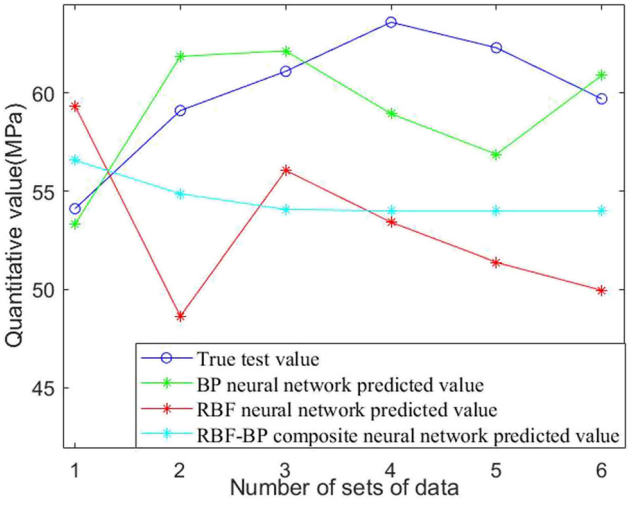


**Figure 4:** Compressive strength predicted results of three neural networks.

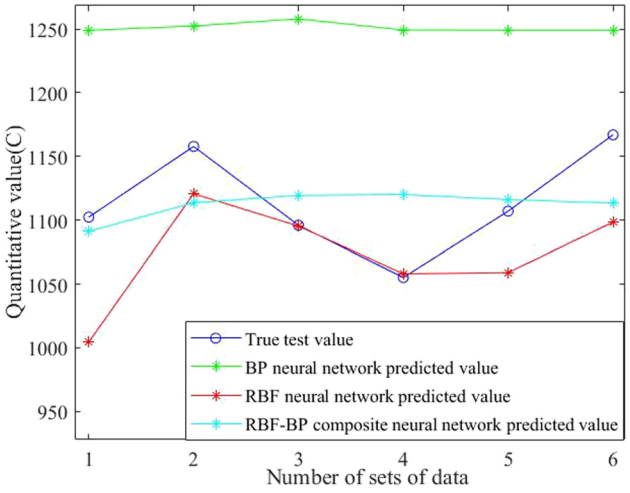


**Figure 5:** Predicted results of three neural networks against chloride ion penetration.

In general, MSE, RMSE, and MAE have a positive correlation, and the smaller the MSE, RMSE, and MAE, the better is the prediction effect, the higher is the prediction accuracy, and the more stable is the prediction data. Among the above three neural network models, compared with the errors of the RBF neural network, the RBF–BP composite neural network model is significantly smaller, and the errors of BP neural network model are largest. In terms of fitting ability, the RBF–BP composite neural network fits best, and the BP neural network has the worst effect. Furthermore, the RBF–BP neural network has a better learning ability and faster convergence speed. In summary, combined with two single neural network models, the RBF–BP composite neural network model has a greater prediction effect than before, and the performance of the RBF–BP composite neural network is considerably better than that of the other two types of neural networks. All three types of neural networks have small error and good predicted effect. The above conclusions are similar to those obtained from previous studies on BP network, RBF network, and RBF–BP network [72–74], and the three types of neural networks are compared and supplemented by previous studies. Meanwhile, this study applies the three kinds of neural networks to geopolymer mortar merging PVA fiber and NS.

**Table 6:** Comparison of evaluation indices of each neural network model

| Neural network models | MSE | RMSE | MAE |
|---|---|---|---|
| BP neural network | 0.014563 | 0.12068 | 0.12068 |
| RBF neural network | 0.0023757 | 0.048741 | 0.037715 |
| RBF–BP composite neural network | 0.00071943 | 0.026822 | 0.026822 |

Comparative analysis of the predicted values revealed that the predicted values of the compressive strength and chloride ion permeation resistance of geopolymer mortar merging PVA fiber and NS by the above three neural networks are in line with the actual situation and meet the requirements for the prediction of compressive strength and chloride ion permeation resistance index electric flux values, thereby possibly providing guidance for the study of the mechanical properties and chloride ion permeation resistance of geopolymer mortar merging PVA fiber and NS. The results of the aforementioned three neural network models can provide guidance for further experiments and engineering studies on the mechanical properties and chloride ion permeation resistance of geopolymer mortars merging PVA fibers and NS.

## 5 Conclusion

1) BP neural networks use the gradient descent method to reduce errors and correct the weight matrix during the training process, requiring several iterations, a slow convergence speed, and a long convergence time. Simultaneously, the BP neural network requires many experiments when selecting neurons in the hidden layer, which is a tedious process. However, the MSE is only 0.014563, which is small and meets the accuracy requirements, and the predicted results are close to the experimental results, with good network generalization ability.
2) The RBF–BP composite neural network couples the advantages of the other two types of neural networks and adopts a double hidden layer structure, having features wherein the BP neural network can solve nonlinear problems and the RBF neural network has a fast convergence rate. Among the three neural networks, the RBF–BP composite neural network fits the best and makes the most accurate prediction.
3) According to the comparison analysis of the assessment results of the three types of neural networks with the real values, the RBF–BP composite neural network model can accurately and effectively predict the compressive strength and chloride ion permeability resistance index electric flux values, and the prediction results fit the real results to a high degree, and the dispersion degree was small. The RBF–BP composite neural network can provide effective guidance for the prediction of the compressive strength and chloride

ion permeation resistance of geopolymer mortars merging PVA fibers and NS.

**Funding information:** The authors would like to acknowledge the financial support received from National Natural Science Foundation of China (Grant No. 51979251, U2040224), Natural Science Foundation of Henan (Grant No. 212300410018), Program for Innovative Research Team (in Science and Technology) in University of Henan Province of China (Grant No. 20IRTSTHN009), and National Innovation and Entrepreneurship Training Program for College Students (Grant No. 202110459175).

**Author contributions:** All authors have accepted responsibility for the entire content of this manuscript and approved its submission.

**Conflict of interest:** The authors state no conflict of interest.

# References

[1] Zhang P, Zhang H, Cui G, Yue X, Guo J, Hui D. Effect of steel fiber on impact resistance and durability of concrete containing nano-$SiO_2$. Nanotechnol Rev. 2021;10(1):504–17.
[2] Ling Y, Zhang P, Wang J, Taylor P, Hu S. Effects of nanoparticles on engineering performance of cementitious composites reinforced with PVA fibers. Nanotechnol Rev. 2020;9(1):504–14.
[3] Shahmansouri AA, Akbarzadeh B, Ghanbari S. Compressive strength prediction of eco-efficient GGBS-based geopolymer concrete using GEP method. J Build Eng. 2020;31:101326.
[4] Hu W, Ma Y, Koehler M, Gong H, Huang B. Mix design optimization and early strength prediction of unary and binary geopolymer from multiple waste streams. J Hazard Mater. 2021;403:123632.
[5] Golewski GL. Green concrete based on quaternary binders with significant reduction in $CO_2$ emissions. Energies. 2021;14(15):4558.
[6] Wang L, Lu X, Liu L, Xiao J, Zhang G, Guo F, Li L. Influence of MgO on the hydration and shrinkage behavior of low heat Portland cement-based materials via pore structural and fractal analysis. Fractal Fract 2022;6:247.
[7] Zhang P, Wang KX, Wang J, Guo JJ, Ling YF. Macroscopic and microscopic analyses on mechanical performance of metakaolin/fly ash based geopolymer mortar. J Clean Prod. 2021;294:126193.
[8] Darvish P, Alengaram UJ, Alnahhal AM, Poh YS, Ibrahim S. Enunciation of size effect of sustainable palm oil clinker sand on the characteristics of cement and geopolymer mortars. J Build Eng. 2021;44:103335.
[9] Zhang P, Wang KX, Wang J, Guo JJ, Hu SW, Ling YF. Mechanical properties and prediction of fracture parameters of geopolymer/alkali-activated mortar modified with PVA fiber and nano-$SiO_2$. Ceram Int. 2020;46(12):20027–37.
[10] Zhang P, Gao Z, Wang J, Guo JJ, Hu SW, Ling YF. Properties of fresh and hardened fly ash/slag based geopolymer concrete: a review. J Clean Prod. 2020;270:122389.
[11] Chithambaram SJ, Kumar S, Prasad MM. Thermo-mechanical characteristics of geopolymer mortar. Constr Build Mater. 2019;213:100–8.
[12] Bingol S, Bilim C, Atis CD, Durak U. Durability properties of geopolymer mortars containing slag. IJST-T Civ Eng. 2020;44(1):561–9.
[13] Elyamany HE, Abd EAM, Elshaboury AM. Magnesium sulfate resistance of geopolymer mortar. Constr Build Mater. 2018;184:111–27.
[14] Liu X, Peng ZC, Pan CH, Hu X, Wan CJ, Yang HY. Mechanical properties and microscopic analysis of nano-silica modified fly ash geopolymer. Mater Rev. 2020;34(11B):22078–82.
[15] Szostak B, Golewski GL. Improvement of strength parameters of cement matrix with the addition of siliceous fly ash by using nanometric C-S-H seeds. Energies. 2020;13(24):6734.
[16] Szostak B, Golewski GL. Effect of nano admixture of CSH on selected strength parameters of concrete including fly ash. IOP Conf Ser: Mater Sci Eng. 2019;416:012105.
[17] Zhang P, Sha DH, Li QF, Zhao SK, Ling YF. Effect of nano silica particles on impact resistance and durability of concrete containing coal fly ash. Nanomater Basel. 2021;11(5):1296.
[18] Wang L, Guo FX, Yang HM, Wang Y. Comparison of fly ash, PVA fiber, MgO and shrinkage-reducing admixture on the frost resistance of face slab concrete via pore structural and fractal analysis. Fractals. 2021;29(2):2140002.
[19] Szostak B, Golewski GL. Rheology of cement pastes with siliceous fly ash and the CSH nano-admixture. Mater. 2021;14(13):3640.
[20] Wu LS, Lu ZH, Zhuang CL, Chen Y, Hu RH. Mechanical properties of nano $SiO_2$ and carbon fiber reinforced concrete after exposure to high temperatures. Mater. 2019;12(22):3373.
[21] Zidi Z, Ltifi M, Zafar I. Synthesis and attributes of nano-$SiO_2$ local metakaolin-based geopolymer. J Build Eng. 2021;33:101586.
[22] Phoo-ngernkham T, Chindaprasirt P, Sata V, Hanjitsuwan S, Hatanaka S. The effect of adding nano-$SiO_2$ and nano-$Al_2O_3$ on properties of high calcium fly ash geopolymer cured at ambient temperature. Mater Des. 2014;55:58–65.
[23] Zhang P, Wang J, Li QF, Wan JY, Ling YF. Mechanical and fracture properties of steel fiber-reinforced geopolymer concrete. Sci Eng Compos Mater. 2021;28(1):299–313.
[24] Ali S, Sheikh MN, Hadi MNS. Behavior of axially loaded plain and fiber-reinforced geopolymer concrete columns with glass fiber-reinforced polymer cages. Struct Conceret. 2021;22(3):1800–16.
[25] Gao Z, Zhang P, Wang J, Wang K. Interfacial properties of geopolymer mortar and concrete substrate: effect of polyvinyl alcohol fiber and nano-$SiO_2$ contents. Constr Build Mater. 2022;315:125735.
[26] Xu F, Deng X, Peng C, Zhu J, Chen JP. Mix design and flexural toughness of PVA fiber reinforced fly ash-geopolymer composites. Constr Build Mater. 2017;150:179–89.

[27] Malik MA, Sarkar M, Xu SL, Li QH. Effect of PVA/$SiO_2$ NPs additive on the structural, durability, and fire resistance properties of geopolymers. Appl Sci Basel. 2019;9(9):1953.
[28] Gao Z, Zhang P, Guo J, Wang K. Bonding behavior of concrete matrix and alkali-activated mortar incorporating nano-$SiO_2$ and polyvinyl alcohol fiber: theoretical analysis and prediction model. Ceram Int. 2021;47(22):31638–49.
[29] Zhang P, Gao Z, Wang J, Wang KX. Numerical modeling of rebar-matrix bond behaviors of nano-$SiO_2$ and PVA fiber reinforced geopolymer composites. Ceram Int. 2021;47(8):11727–37.
[30] Hu C, Chen P, Zhang XP, Xiang WH, Liu RJ, Tian Y. Investigating on chloride ion and sulfate corrosion resistance of different steel phase cements. Concrete. 2020;10:98–101.
[31] Wang L, Luo R, Zhang W, Jin M, Tang S. Effects of fineness and content of phosphorus slag on cement hydration, permeability, pore structure and fractal dimension of concrete. Fractals. 2021;29(2):2140004.
[32] Wang WC. Study on durability of nano-particles and fiber reinforced geopolymer mortar. Dissertation. Zhengzhou: Zhengzhou University; 2020.
[33] Liu QF, Iqbal MF, Yang J, Lu XY, Zhang P, Rauf M. Prediction of chloride diffusivity in concrete using artificial neural network: Modelling and performance evaluation. Constru Build Mater. 2021;268:121082.
[34] Yang T, Yao X, Zhang ZH. Quantification of chloride diffusion in fly ash-slag-based geopolymers by X-ray fluorescence (XRF). Construct Build Mater. 2014;69:109–15.
[35] Wang KX, Zhang P, Guo JJ, Gao Z. Single and synergistic enhancement on durability of geopolymer mortar by polyvinyl alcohol fiber and nano-$SiO_2$. J Mater Res Technol. 2021;15:1801–14.
[36] Golewski GL. Validation of the favorable quantity of fly ash in concrete and analysis of crack propagation and its length - Using the crack tip tracking (CTT) method - In the fracture toughness examinations under Mode II, through digital image correlation. Construct Build Mater. 2021;296:122362.
[37] Golewski GL. Evaluation of fracture processes under shear with the use of DIC technique in fly ash concrete and accurate measurement of crack paths lengths with the use of a new crack tip tracking method. Measurement. 2021;181:109632.
[38] Nagajothi S, Elavenil S. Influence of aluminosilicate for the prediction of mechanical properties of geopolymer concrete - artificial neural network. Silicon-neth. 2020;12(5):1011–21.
[39] Rahman SK, Al-Ameri R. Experimental investigation and artificial neural network based prediction of bond strength in self-compacting geopolymer concrete reinforced with basalt FRP bars. Appl Sci-Basel. 2021;11(11):4889.
[40] Asteris PG, Apostolopoulou M, Skentou AD, Moropoulou A. Application of artificial neural networks for the prediction of the compressive strength of cement-based mortars. Comput Concrete. 2019;24(4):329–45.
[41] Onal O, Ozturk AU. Artificial neural network application on microstructure-compressive strength relationship of cement mortar. Adv Eng Softw. 2010;41(2):165–9.
[42] Abdelhedi M, Jabbar R, Mnif T, Abbes C. Prediction of uniaxial compressive strength of carbonate rocks and cement mortar using artificial network and multiple linear regressions. Acta Geodyn Geomater. 2020;17(3):367–77.
[43] Ling YF, Wang KJ, Wang XH, Li WG. Prediction of engineering properties of fly ash-based geopolymer using artificial neural networks. Neural Comput Appl. 2021;33(1):85–105.
[44] Bhogayata A, Kakadiya S, Makwana R. Neural network for mixture design optimization of geopolymer concrete. Aci Mater J. 2021;118(4):91–6.
[45] Aneja S, Sharma A, Gupta R, Yoo DY. Bayesian regularized artificial neural network model to predict strength characteristics of fly-ash and bottom-ash based geopolymer concrete. Mater. 2021;14(7):1729.
[46] Gunasekara C, Atzarakis P, Lokuge W, Law DW, Setunge S. Novel analytical method for mix design and performance prediction of high calcium fly ash geopolymer concrete. Polymers Basel. 2021;13(6):900.
[47] John SK, Cascardi A, Nadir Y, Aiello MA, Girija K. A new artificial neural network model for the prediction of the effect of molar ratios on compressive strength of fly ash-slag geopolymer mortar. Adv Civ Eng. 2021;2021:6662347.
[48] Nazari A, Sanjayan JG. Modelling of compressive strength of geopolymer paste, mortar and concrete by optimized support vector machine. Ceram Int. 2015;41(9):12164–77.
[49] Li XH, Zhang T, Deng Z, Wang J. Preparation and mechanical properties of a base polymer of metakaolin: A recognition method of plate shape defect based on RBF–BP neural network optimized by genetic algorithm. 26th Chinese Control and Decision Conference; 2014: p. 3992–6.
[50] Liu GH. A new method for fault diagnosis of building electrical system based on RBF–BP neural network. ICICAS; 2019: p. 470–4.
[51] Han D, Che YX, Song P, Wang Q. Preparation and mechanical properties of a base polymer of metakaolin. Sichuan Cement. 2009;168(1):44–50.
[52] Apha S, Prinya C, Kedsarin P. Workability and strength of lignite bottom ash geopolymer mortar. J Hazard Mater. 2009;168(1):44–50.
[53] Sun S. Adjustment and calculation of water glass modulus. Mine Construct Technol. 1984;2:26–9.
[54] Zhang P, Han X, Zheng YX, Wan JY, Hui D. Effect of PVA fiber on mechanical properties of fly ash-based geopolymer concrete. Rev Adv Mater Sci. 2021;60(1):418–37.
[55] Shen H, Wang ZX, Gao CY, Qin J, Yao FB, Xu W. Determining the number of BP neural network hidden layer units. J Tianjin Univ Technol. 2008;05:13–5.
[56] Hu X. Prediction of high performance concrete strength based on artificial neural network. Changsha, China: Hunan University; 2014.
[57] Drioli C, Rocchesso D. Orthogonal least squares algorithm for the approximation of a map and its derivatives with a RBF network. Signal Progress. 2003;83(2):283–96.
[58] Hartman EJ, Keeler JD, Kowalski JM. Layered neural networks with Gaussian hidden units as universal approximations. Neural Comput. 1990;2:210–25.
[59] Yi ZM, Deng ZD, Qin JZ, Liu Q, Du D, Zhang DS. $NO_x$ prediction of sintering flue gas based on RBF–BP hybrid neural network. J Iron Steel Res. 2020;32(7):639–46.
[60] Wen H, Xie WX, Pei JH. A structure-adaptive hybrid RBF–BP classifier with an optimized learning strategy. PLoS One. 2016;11(10):164719.

[61] Yi Z, Qin J, Deng Z, Liu Q. Prediction $NO_x$ emission from sintering plant with a radial basis function and back propagation hybrid neural network. Int J Environ Sci Technol. 2021. doi: 10.1007/s13762-021-03379-y.
[62] Assaedi H, Alomayri T, Siddika A, Shaikh F, Alamri H, Subaer S, et al. Effect of nanosilica on mechanical properties and microstructure of PVA fiber-reinforced geopolymer composite (PVA-FRGC). Mater. 2019;12(21):3624–35.
[63] Tavakoli D, Dehkordi RS, Divandari H, De BJ. Properties of roller-compacted concrete pavement containing waste aggregates and nano $SiO_2$. Construct Build Mater. 2020;249:118747.
[64] Li G, Zhou JC, Yue J, Gao X, Wang KJ. Effects of nano-$SiO_2$ and secondary water curing on the carbonation and chloride resistance of autoclaved concrete. Construct Build Mater. 2020;235:117465.
[65] Sun JF, Shen XD, Tan G, Tanner JE. Modification effects of Nano-$SiO_2$ on early compressive strength and hydration characteristics of high-volume fly ash concrete. J Mater Civ Eng. 2019;31(6):04019057.
[66] Sun HF, Li ZSS, Memon SA, Zhang QW, Wang YC, Liu B, et al. Influence of ultrafine $2CaO{\cdot}SiO_2$ powder on hydration properties of reactive powder concrete. Mater. 2015;8(9):6195–207.
[67] Liu FY, Xu K, Ding WQ, Qiao YF, Wang LB. Microstructural characteristics and their impact on mechanical properties of steel-PVA fiber reinforced concrete. Cement Concrete Compos. 2021;123:104196.
[68] Guo L, Wu YY, Xu F, Song XT, Ye JY, Duan P, et al. Sulfate resistance of hybrid fiber reinforced metakaolin geopolymer composites. Compos Part B-Eng. 2020;183:107689.
[69] Batista RP, Trindade ACC, Borges PHR, Silva FD. Silica fume as precursor in the development of sustainable and high-performance MK-based alkali-activated materials reinforced with short PVA fibers. Front Mater. 2019;6:77.
[70] Xu SL, Malik MA, Qi Z, Huang BT, Li QH, Sarkar M. Influence of the PVA fibers and $SiO_2$ NPs on the structural properties of fly ash based sustainable geopolymer. Construct Build Mater. 2018;164:238–45.
[71] Xiao SH, Liao SJ, Zhong GQ, Guo YC, Lin JX, Xie ZH, et al. Dynamic properties of PVA short fiber reinforced low-calcium fly ash-slag geopolymer under an SHPB impact load. J Build Eng. 2021;44:103220.
[72] Li H, Peng T. Prediction of concrete compression strength based on BP and PBF neural network theories. J Wuhan Univ Technol. 2009;31(8):33–6.
[73] Li N, Zhao JH, Wang J, Zhu Q. Prediction of hybrid fiber reinforced concrete strength on base of RBF & BP. Adv Mater Res. 2014;1035:180–5.
[74] Zou H, Zhou YH, Wang L, Zhang ZY. Maximum temperature prediction of concrete pouring storehouse of high arch dam based on RBF–BP neural network model. Water Res Pwr. 2016;34(3):67–9.